JOURNAL OF CATALYSIS **179,** 390–399 (1998)
ARTICLE NO. CA982231

Pd-Mn Silica Supported Catalysts

1. Formation of the Bimetallic Particles

A. J. Renouprez,[1] J. F. Trillat, B. Moraweck, J. Massardier, and G. Bergeret

Institut de Recherches sur la Catalyse, CNRS, 2 Avenue A. Einstein, F69626, Villeurbanne Cedex, France

Received January 22, 1998; revised June 20, 1998; accepted July 4, 1998

The synthesis of Pd-Mn silica-supported catalysts from bis-acetylacetonates precursors is described. EXAFS and X-ray diffraction lead to a clear understanding of the mode of fixation of the two complexes on the silica surface. Whereas $Pd(acac)_2$ forms large crystals, weakly interacting with the support, the Mn complex undergoes a partial decomposition, leading to a molecular layer of $Mn(acac)_x$. The decomposition of these precursors followed by thermal methods confirms a marked difference in the mode of interaction between the silanol groups of the support and the two acetylacetonate complexes. After activation of these precursors, TEM and analytical microscopy provide a picture of the distribution of palladium and manganese on the support. Manganese, for the most part, is spread in the form of a thin layer of oxide over the silica surface. The remaining part is incorporated in 3–6-nm bimetallic Pd-Mn particles, as shown by EXAFS experiments performed at the palladium K-edge. The comparison of EXAFS and EDX results indicates that the alloy particles are partly surrounded by manganese oxide.

Key Words: **palladium acetylacetonate; manganese acetylacetonate; Pd-Mn bimetallic; Pd-Mn alloy; EXAFS.**

1. INTRODUCTION

The association of palladium or platinum with a less electronegative metal like Cr, Co, or Mn is expected to modify the electronic properties of the noble metal. This was shown with Pd-Cr (1) and more recently with Pt-Mn (2). In both cases, the presence of the second element was shown to favor the CO-NO conversion. Actually, in these two bimetallic associations, a large fraction of the second metal remains in the oxidic form. In the case of the Pd-Cr catalyst, we have shown by EXAFS that, besides the oxide phase, 10 to 15% of the chromium is in interaction with palladium (1). In the present study, the metallic couple under investigation is Pd-Mn, for which a strong electronic interaction between the two elements is also expected because of a still larger difference in electronegativity. Indeed, we have shown (3) that this bimetallic catalyst is very efficient for CO-NO conversion, lowering the light-off temperature of the NO reduction by 60°C.

To prepare these catalysts, we have used precursors which can lead, in some cases, to well-defined mixed complexes. For example, it has been shown recently (4) that mixed PdCu bis-acetylacetonates are obtained by slow evaporation on the support of a mixture of the toluene solutions of the two complexes. After decomposition under argon of these crystalline complexes, homogeneous Pd-Cu microcrystalline alloys were obtained in the whole Pd/Cu composition range. In the present case, the same preparation procedure as for Pd-Cu has been employed, even if with this couple, because of the low reducibility of Mn, there is little hope to obtain at once an homogeneous alloy.

The purpose of this study is to establish the mechanism of fixation of the complexes on the support and of their decomposition, using thermal methods and X-ray absorption. After activation of the precursors, the location on the support of the various elements has been determined with the help of analytical microscopy and the formation of alloys with EXAFS.

2. EXPERIMENTAL

2.1. Catalyst Preparation

Palladium(II) and manganese(II) bis-acetylacetonates $Pd(C_5H_7O_2)_2$ and $Mn(C_5H_7O_2)_2$ (1 g) from Aldrich Chemical are dissolved in respectively 100 and 200 ml of toluene at 350 K. Amounts of these solutions necessary to reach a total metal weight concentration of 2 to 3% are added to 5 g of Degussa Aerosil 200 silica. After stirring for 24 h at 300 K, the slurry is filtered and dried in vacuum at 330 K. The chemical analysis shows that in this exchange procedure, 20% of the Pd complex and 80% of the Mn complex are fixed on the support. This has been taken into account to reach the requested Pd/Mn ratio. The compositions of the catalysts determined by chemical analysis are gathered in Table 1.

[1] To whom correspondence should be addressed. E-mail: renouprez@catalyse.univ-lyon1.fr.

0021-9517/98 $25.00

TABLE 1

Composition of the Catalysts

Sample	Composition (wt%) Pd	Mn	Composition (at%) Pd
Pd/SiO_2	2.00	—	100
$Pd_{90}Mn_{10}/SiO_2$	1.78	0.10	90.2
$Pd_{65}Mn_{35}/SiO_2$	1.41	0.39	65.1
Mn/SiO_2	—	3.20	0

2.2. Thermal Methods

The decomposition of the organometallic precursors was followed by TDA-TG analysis with a SETARAM 92 instrument. The masses corresponding to H_2 (2), H_2O (18), CO_2 (44), CH_3CO^+ (43), and CH_3COCH_3 (58) were also simultaneously analysed by mass spectroscopy.

The sample (15–20 mg) was introduced into the thermogravimetric apparatus to measure the temperature of the ligand elimination during heating under helium. In a second experiment, the reduction under a mixture $N_2 + H_2$ (1%) was followed as well. The temperature was raised from 370 to 870 K at 10 K/min. Between treatments, the samples were flowed with dry N_2 at 300 K for 1 h.

Additional thermodesorption experiments have finally been performed in an UHV instrument equipped with ionic pumps (nominal pressure 10^{-6} Pa) and in which detection is achieved by a Micromass PC spectrometer from VG Instruments. The purpose is to measure with good accuracy the evolution of the species of mass 100 corresponding to $C_5H_8O_2$.

2.3. X-Ray Diffraction and Electron Microscopy

The crystallisation on the support of the organometallic compounds and the formation of the metallic phases were followed by powder X-ray diffraction using two instruments. For the study of the deposition of the precursors, a classic Philips diffractometer equipped with a graphite monochromator placed before the scintillation detector was sufficient.

The formation of the metallic phase was followed by *in situ* diffraction in a previously described instrument (5), including an oven into which different gases can be flowed. The detection is achieved by a position-sensitive detector, which improves the sensitivity by more than one order of magnitude but slightly degrades the angular resolution.

The granulometry of the particles was determined with a JEOL JEM 2010 electron microscope. Surface-averaged mean diameters d_s were determined using the classical expression

$$d_s = \sum n_i d_i^3 \Big/ \sum n_i d_i^2,$$

where n_i is the number of particles with the diameter d_i.

The composition of individual particles was determined with an energy-dispersive device composed of a Si-Li detector by measuring the intensity of the Lα and Kα emissions of Pd and Mn at 2.84 keV and 5.90 keV, respectively.

The analysis of the smallest particles can be achieved by reducing the size of the probed area to 1 nm^2. A mean composition X_M was evaluated from the expression:

$$X_M = \sum X_i n_i d_i^3 \Big/ \sum n_i d_i^3,$$

where n_i is the number of particles with the composition X_i and diameter d_i.

As shown in a recent study by this technique of the Pd-Pt system (6), the statistical error on the measurement is of the order of 10%, both because of the small number of atoms hit by the focused electron beam and by the limitation of the time of measurement. It was also shown that increasing the time of analysis on the same particle can produce a preferential sputtering of the most volatile metal, specially if it is located at the surface of the particles.

2.4. X-ray Absorption Experiments

The experiments were performed at the LURE-DCI facility on the XAS4 station. For the experiments in transmission mode at the Pd K-edge, the optics was composed of a Ge (400) double crystal monochromator and the detection performed with Kr filled ion chambers. In these conditions, the minimum step in energy was 3 eV, the energy being calibrated at the half edge jump at 24350 eV, with a 15-μm thick metal foil from Goodfellow. The transmission mode was chosen to perform EXAFS experiments on the supported and unsupported Pd acetylacetonate complexes.

At the Mn K-edge, only XANES spectra were recorded on the bimetallic catalysts. They were carried out with a Si (311) double crystal monochromator to improve the energy resolution, followed by a double glass mirror to eliminate the high order harmonics. Fluorescence mode was preferred to transmission because of the high absorption of palladium and silica at low energy. The monochromator was calibrated at the first inflection point of the absorption jump (6359 eV), corresponding to the $1s \rightarrow 3d$ transition, with a 4-μm thick foil from Goodfellow. The detection was performed with a scintillation detector; Fe filters (20-μm thick) were inserted between the sample and the detector to reduce the number of elastic photons and enhance the contrast. The spectra were recorded over 100 eV in steps of 0.2 eV. The transmission mode was chosen to perform EXAFS experiments on the supported and unsupported Mn acetylacetonate complexes using air-filled ion chambers.

For each edge the counting time ranged from 1 s to 20 s, depending on the detection mode and the type of experiment (XANES or EXAFS). The EXAFS spectra were recorded over 1000 eV in steps of 3 eV; 4 to 10 spectra

were summed before a complete analysis carried out with homemade software, following the method described in several previous works (1, 5, 7). The modeling of reduced EXAFS data was performed by the flexible simplex method (8) by optimizing the four main parameters, n, R, $\Delta\sigma$, and ΔE_0 and by computing a merit factor expressed as

$$Q = \frac{\sum[k^3 \cdot |\chi_{\text{exp}}(k)| - k^3 \cdot |\chi_{\text{cal}}(k)|]^2}{\sum[k^3 \cdot |\chi_{\text{exp}}(k)|]^2},$$

allowing the comparison between various fits in the case of the bimetallic catalysts at the Pd K-edge. The precision on the determination of n and R is 10% and 0.02 Å, respectively.

The maximum number of parameters, N, depends on the Δk and ΔR ranges chosen in the reciprocal and direct space, respectively. Following the Shannon criterion, it is given by the relationship (9):

$$N_{\text{max}} = \frac{2\Delta k \Delta R}{\pi} + 2.$$

Experimental backscattering amplitudes and phase-shifts were extracted from measurements on metal foils for the Pd-Pd and Mn-Mn pairs (15 and 4 μm, respectively). Concerning the metal–oxygen pairs, these functions were determined from experiments on PdO and MnO purchased from Johnson Matthey. In the case of the Pd–Mn pairs, these functions have been computed with the FEFF6 code (10) using the crystallographic data of the cc PdMn ordered phase (11) in which the Pd–Mn distance is 2.7115 Å.

The samples were placed in an oven following the design of Lytle *et al.* (12), for the studies in transmission mode. Treatments identical to those employed during the preparation were applied in the EXAFS cell and the spectra were recorded at 300 K, under H_2 in the case of the calcination/reduction procedure or under He for samples submitted to a simple decomposition under rare gas. Finally the experiments performed in fluorescence were done in a second oven adapted to the reflection geometry, allowing the same type of treatments.

3. RESULTS AND DISCUSSION

3.1. Chemical Exchange of the Precursors on the Silica Support

As mentioned above, the presence of $Mn(acac)_2$ in the solution lowers the exchange capacity for the Pd complex, as can be seen in Fig. 1. After exchange with the support and drying at 330 K, the two complexes exhibit different diffractograms, shown in Figs. 2a and 2b. It can be observed in Fig. 2a that the widths of the $Pd(acac)_2$ lines are close to the instrumental resolution and therefore correspond to crystals larger than 20 to 30 nm. As mentioned elsewhere (4), the unit cell of the supported complex was found to be identical to that of the starting unsupported compound.

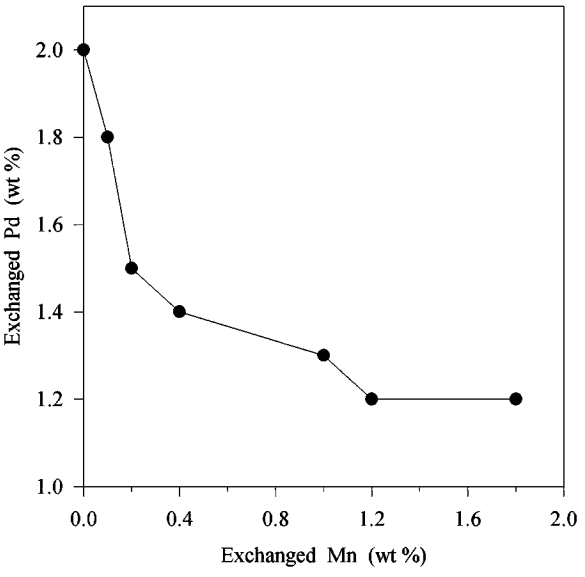

FIG. 1. Illustration of the adsorption competition between the Pd and Mn complexes.

Conversely, the Mn complex, which is also well crystallized in the solid state, was found to be totally amorphous when deposited on the silica. This difference of structure between the two supported complexes is certainly related to differences in the mode of their interaction with the support.

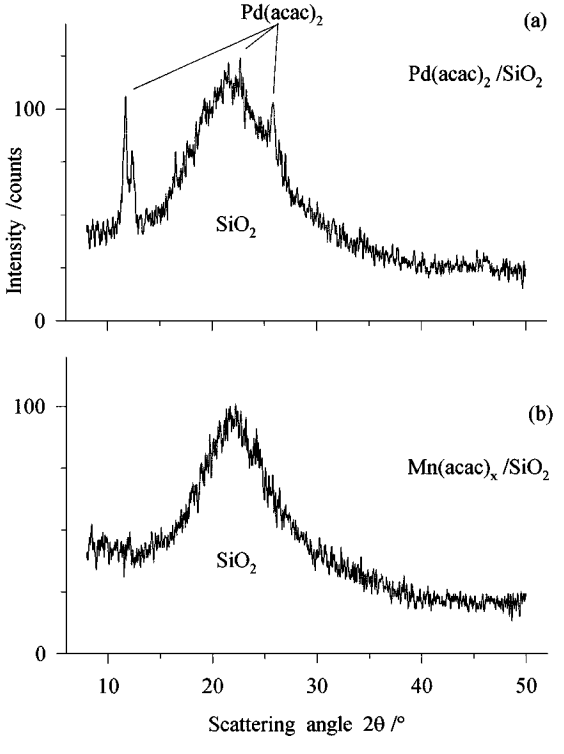

FIG. 2. X-ray diffraction patterns after exchange with silica and drying at 330 K: (a) Pd; (b) Mn.

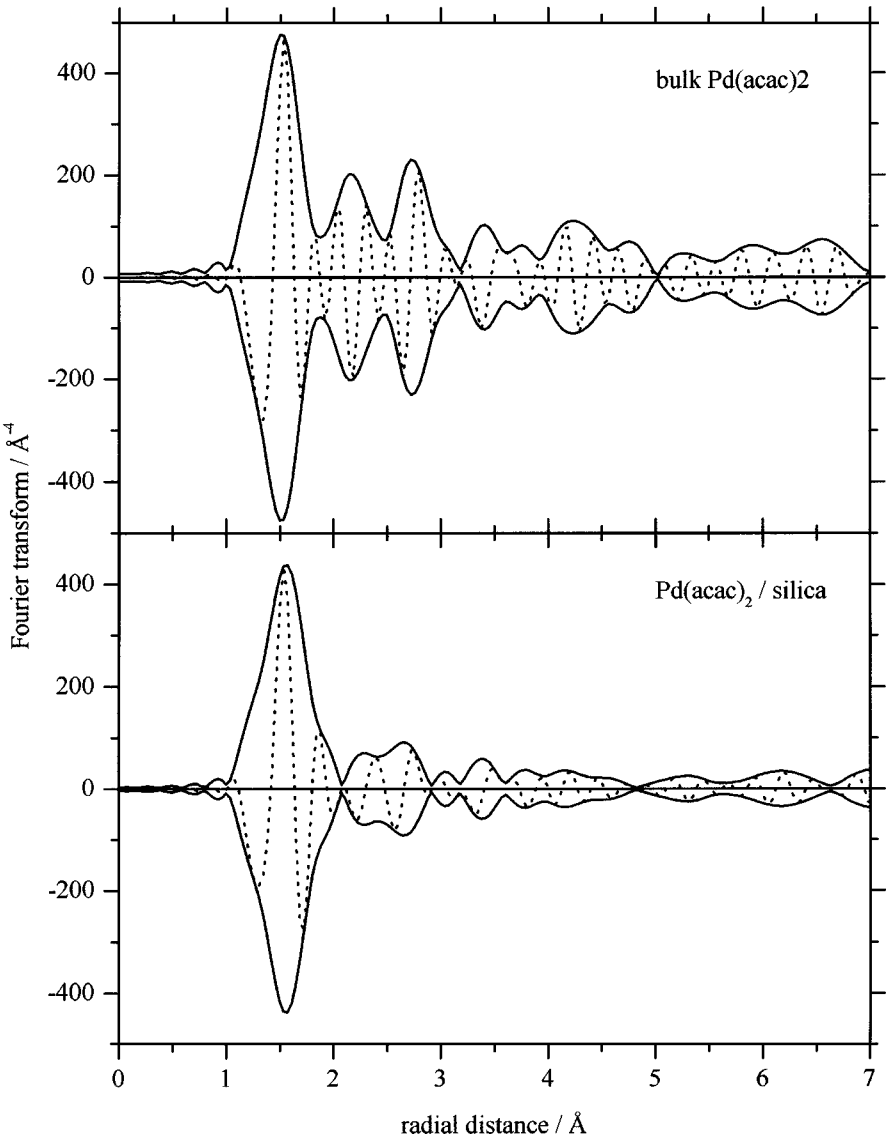

FIG. 3. EXAFS data for Pd complex: magnitude and imaginary part of the FT of bulk and silica exchanged Pd acetylacetonate complex.

To corroborate this assumption, EXAFS experiments over both Mn and Pd K-edges were performed on the unsupported solids and dried silica-supported complexes.

Figure 3 shows the magnitudes and imaginary parts of the Fourier transforms (FT) of the as-purchased and silica-supported Pd complex. In spite of a slight reduction of amplitude of the first peak of the FT corresponding to metal–oxygen distances, a comparison of the modeled and of the experimental EXAFS spectra shown in Fig. 4 leads to the same number of first neighbours. As can be seen in Table 2, four oxygen atoms are found in the first coordination shell of palladium, at a distance close to that found in the crystal, with a slight increase of the Debye–Waller (DW) factor σ.

However, as shown in Fig. 3, the second and third peaks of the FT of the spectrum of the supported sample (Pd-C distances), have a reduced amplitude compared to that of the bulk compound. This could be related to some disorder in the atomic arrangement of the supported $Pd(acac)_2$ unit but suggests a discrepancy between the XRD and EXAFS results, however, since Fig. 2a shows well-defined lines

TABLE 2

EXAFS Characterization of the Supported Complexes

Sample	n	R (Å)	$\Delta\sigma^2$ (Å^2)	Δk (Å^{-1})	ΔR (Å)	Q (%)
Pd $(acac)_2$ bulk	3.9	1.96	0.0004	2.2–14.8	0.96–1.96	10
Pd $(acac)_2/SiO_2$	4.1	1.98	0.0008	2.2–14.8	0.96–1.99	5.0
Mn $(acac)_2$ bulk	4.0	2.16	0.0001	2.4–11.8	1.19–2.15	2.5
Mn $(acac)_x/SiO_2$	3.0	2.20	0.0007	2.4–11.8	1.19–2.19	4.5

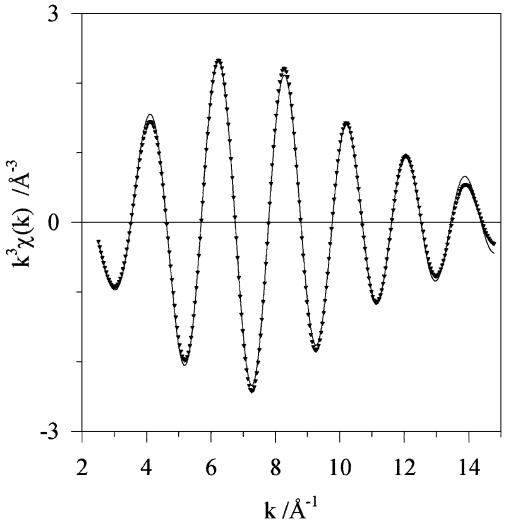

FIG. 4. First shell experimental (triangles) and modeled (solid line) contribution for the exchanged Pd complex.

corresponding to the $Pd(acac)_2$ phase. Actually, besides the crystalline phase leading to narrow lines, the X-ray spectra of the supported complex show an increased background with respect to pure silica. One can thus assume that two forms of $Pd(acac)_2$ may coexist on the carrier surface after the impregnation process. The first one consisting of large crystallites, producing the narrow XRD lines, and the second forming a thin layer covering the carrier, which increases only the XRD pattern background. Consequently, part of the long-range order observed on the FT of the dried precursor has disappeared, leading to the observed decrease of the FT intensity beyond the first coordination sphere.

On the contrary, in Fig. 5, the amplitude of the first peak of the FT of the Mn-supported complex is strongly reduced, compared to that of the bulk compound. Indeed, the number of oxygen atoms surrounding Mn decreases from 4 to 3 after deposition on the silica carrier. Table 2 shows a slight increase of the Mn-O distances and of the DW factor. The excellent fit presented in Fig. 6 corresponds to a merit factor Q of 4.5%. This leads to the idea that a reaction between the Mn complex and one silanol group of silica has occurred, with the elimination of one ligand of the molecule.

3.2. Thermal Decomposition of the Supported Precursors

The supported precursors were heated in an argon flow in the TDA-TGA instrument. As shown by Fig. 7, the decomposition of the $Mn(acac)_2$ begins at 450 K with evolution of water and hydrogen, followed between 500 and 600 K by CH_3CO^+ fragments and finally around 650 K by carbon dioxide. A comparison of the evolution of these acetyl moieties, identified by the 43 mass fragment, is shown in Fig. 8 for the Pd/SiO_2, Mn/SiO_2, and $(Pd_{65}\text{-}Mn_{35})/SiO_2$ catalysts. These curves seem to confirm the greater stability of

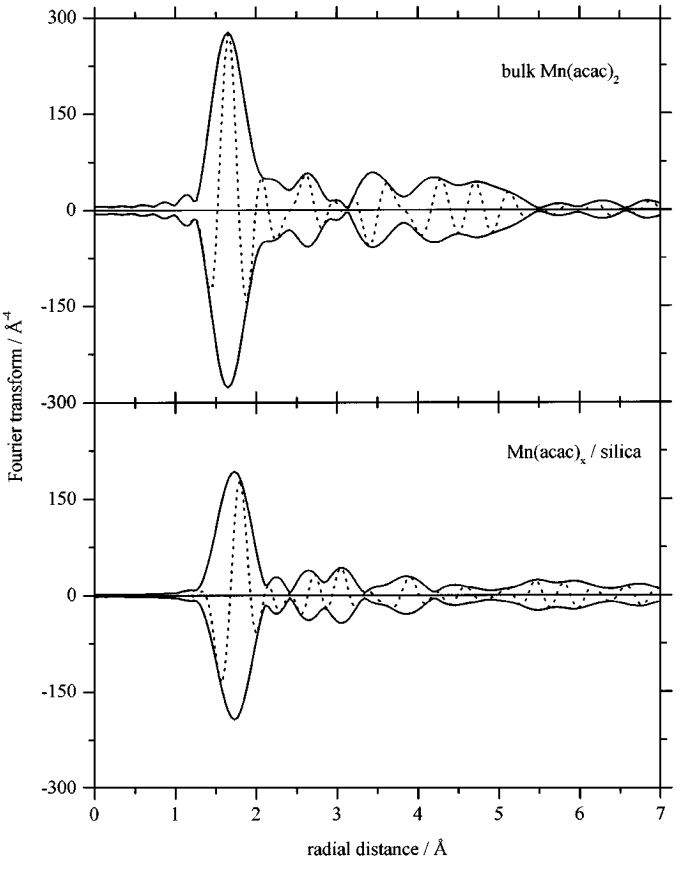

FIG. 5. EXAFS data for Mn complex: magnitude and imaginary part of the FT of bulk and silica exchanged Mn acetylacetonate complex.

the adsorbed Mn complex; indeed, the loss of CH_3CO^+ takes place at 470 K for Pd and between 520 and 670 K for Mn. When both elements are present, the diagram presents a main peak at 520 K and a smaller one at 620 K. One can conclude that the presence of palladium, which, as

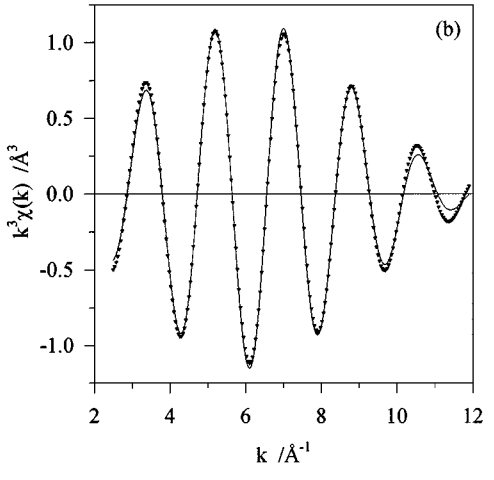

FIG. 6. First shell experimental (triangles) and modeled (solid line) contribution for the exchanged Mn complex.

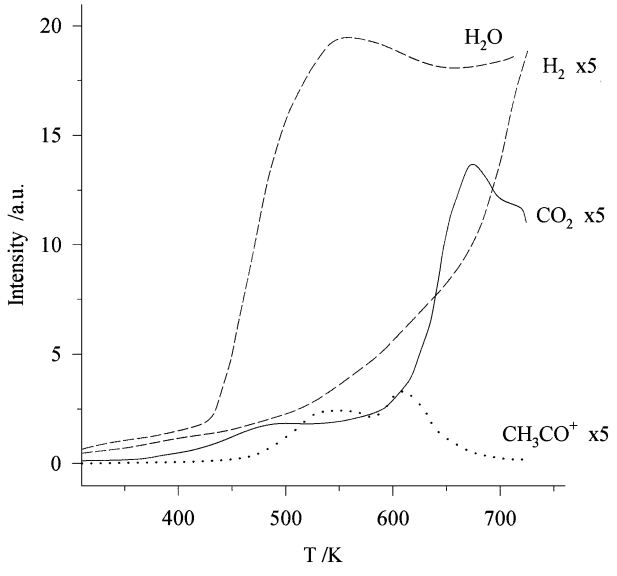

FIG. 7. Mass spectrometry analysis during the decomposition of supported Mn acetylacetonate under argon: from top to bottom masses 18 (H_2O), 2 (H_2), 44 (CO_2) and 43 (CH_3CO^+). The intensity of the three last masses are multiplied by 5.

demonstrated previously (4) undergoes a self-reduction by the evolved hydrogen during this heating, has little influence on the decomposition of the $Mn(acac)_2$ molecules.

Now, if one considers the diagram of Fig. 9 recorded at the 100 mass unit, which corresponds to the evolution of acetylacetone, one concludes that the Mn complex loses one ligand at low temperature, below 400 K, whereas it is only evolved at 550 K in the case of palladium. This corroborates the hypothesis put forward on the basis of the EXAFS results of partial decomposition of the Mn complex by contact with the silica support. This would also agree with a reduction of the coordination number of Mn from 4 to 3; the adsorbed form is formally written:

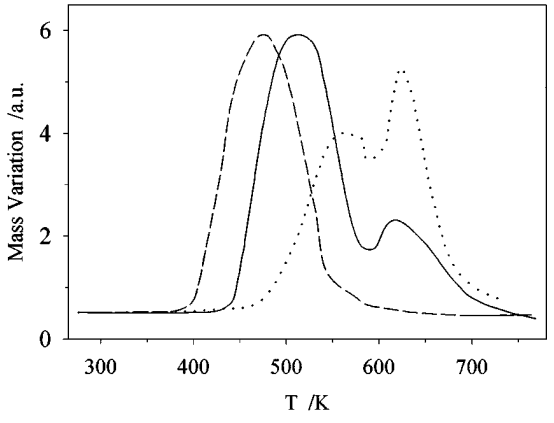

FIG. 8. Evolution of the mass 43 (CH_3CO^+) during the decomposition of supported Pd (dashed line), Mn (dotted line), and (Pd-Mn) (65/35) (full line), acetylacetonates under argon.

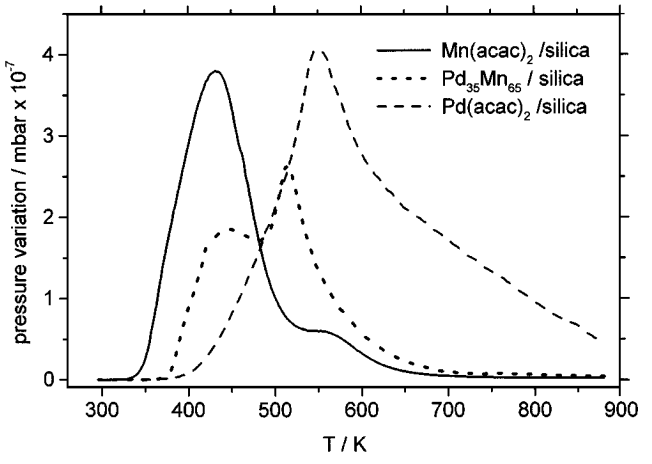

FIG. 9. Evolution of the species corresponding to $C_5H_8O_2$ (mass 100).

$$|{-}OH + Mn(C_5H_7O_2)_2 \Rightarrow |{-}O{-}Mn(C_5H_7O_2) + C_5H_8O_2$$

with the evolution of one acetyl-acetone molecule, probably remaining adsorbed on the silica up to 400 K, a phenomenon already observed in the case of $Pd(C_5H_7O_2)_2$ on alumina (13).

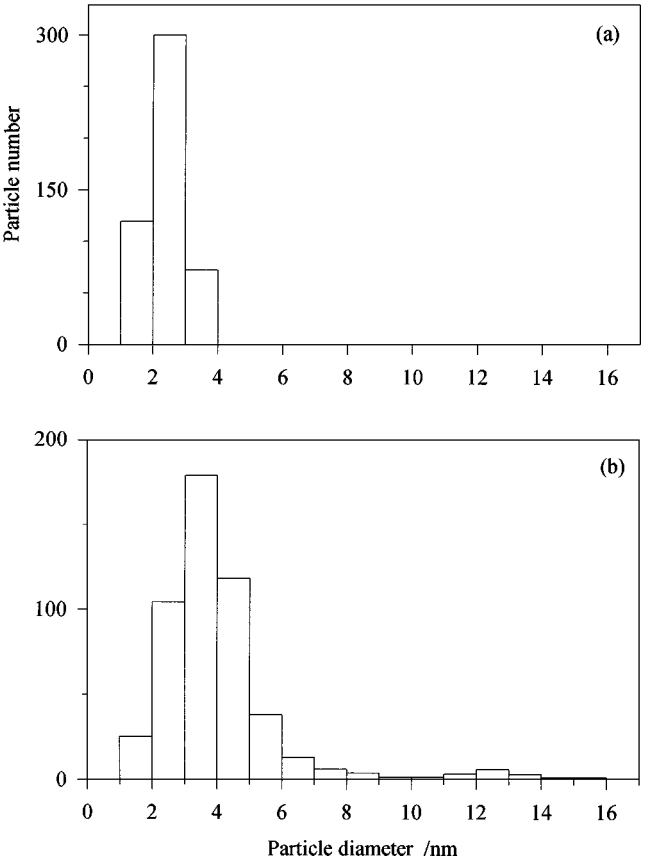

FIG. 10. Distributions of the diameters of the particles for monometallic Pd/SiO_2: (a) heating under argon up to 770 K, $d_s = 2.7$ nm; (b) calcination at 720 K followed by reduction at 870 K, $d_s = 6.7$ nm.

3.3. Formation and Characterization of Bimetallic Particles

3.3.1. Electron microscopy. Two different procedures of decomposition of the precursors were employed: a simple heating under argon up to 770 K, which, as shown by thermal analysis, seems to be sufficient to decompose the organic ligands, or a calcination at 720 K followed by a reduction at 870 K. Actually, this second procedure appeared to be necessary to remove the carbonaceous residues, as it leads to considerably more active catalysts in the CO-NO conversion.

The comparison between the histograms of Figs. 10a and 10b corresponding to the monometallic Pd catalyst submitted to these two types of treatments, shows that the calcination/reduction procedure increases considerably the number of large particles which is illustrated by an augmentation of the mean diameter, d_s, from 2.7 to 6.7 nm. This phenomenon occurs as well on the bimetallic catalysts as observed on the histograms of Figs. 11a and 11b corresponding to the $Pd_{65}Mn_{35}/SiO_2$ catalyst which finally exhibit a dispersion ranging between 25 and 35%.

When analytical microscopy is performed in the scanning mode on a large area on the two bimetallic samples, the

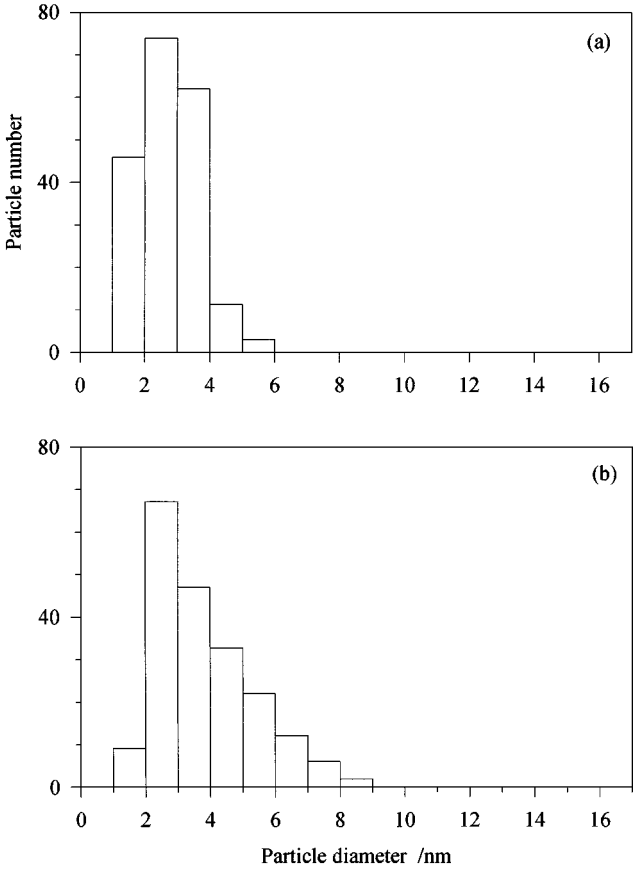

FIG. 11. Distributions of the diameters of the particles for bimetallic $Pd_{65}Mn_{35}/SiO_2$: (a) heating under argon up to 770 K, $d_s = 3.2$ nm; (b) calcination at 720 K followed by reduction at 870 K, $d_s = 4.9$ nm.

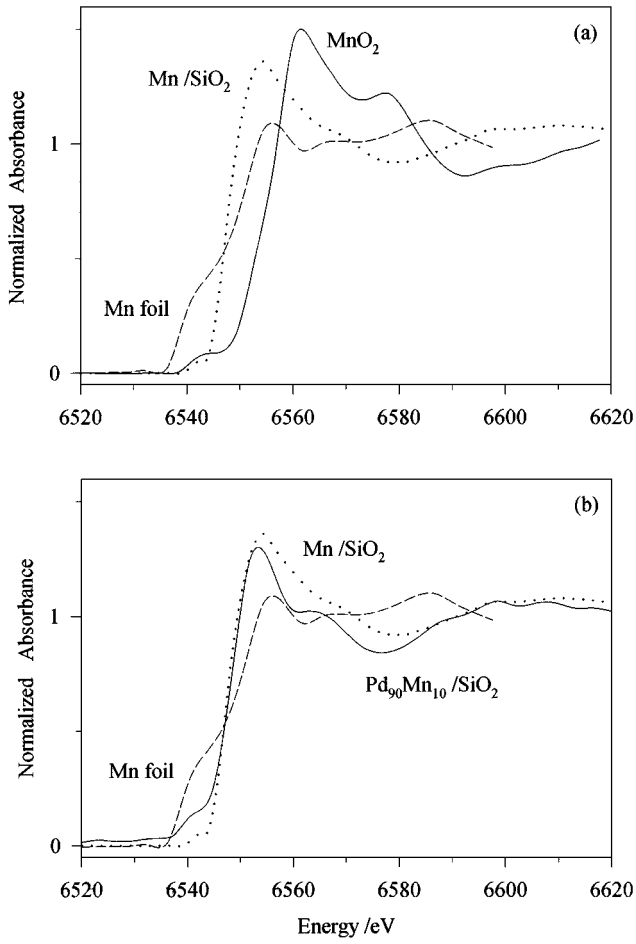

FIG. 12. X-ray absorption edge structure: (a) metallic manganese (dashed line), monometallic catalyst Mn/SiO_2 (dotted line), and manganese oxide MnO_2 (full line); (b) metallic manganese (dashed line), monometallic catalyst Mn/SiO_2 (dotted line), and bimetallic catalyst $Pd_{90}Mn_{10}/SiO_2$ (full line).

Pd/Mn ratio is identical to the value measured by chemical analysis. On the contrary, the analysis of individual particles in the spot mode shows a net deficit in manganese. Actually, all particles which can be observed on the EM pictures contain an excess of palladium; on the other hand, for monometallic manganese (as for the bimetallic catalysts), Mn is dispersed on the support, forming such a thin layer that individual particles are hardly visible.

To determine if Pd and Mn, both present in the particles, are in interaction in the metallic state, it was necessary to perform X-ray absorption experiments.

3.3.2. X-Ray absorption studies. Figure 12a shows a comparison of the XANES at the Mn K-edge, between the reference Mn foil, the monometallic Mn catalyst, after treatment in argon at 770 K, and a reference MnO_2 sample. Although a complete interpretation of these structures is not possible, it can be concluded from the large energy shift between the catalyst and MnO_2 that part of the manganese

in the catalyst is in a lower valence state. No shift is observed on Fig. 12b between the Mn K-edge of the Mn/SiO_2 sample and of the bimetallic $Pd_{90}Mn_{10}/SiO_2$, which discards a net electronic interaction between palladium and manganese. However, the small bump located at 6542 eV, observed on the bimetallic sample and also present on the reference foil, could be the indication of the presence of a small amount of metallic Mn.

The amplitudes and imaginary parts of the FTs of the EXAFS spectra at the Pd K-edge of the two bimetallic catalysts submitted to the calcination/reduction treatment are presented in Fig. 13. The modeling of the first peak of the Fourier transform of the $Pd_{65}Mn_{35}$ catalyst is displayed in Fig. 14a with only Pd atoms, and for comparison, in Fig. 14b after the introduction of Mn atoms in the first coordination shell of the palladium. One notices the clear improvement of the fit, especially in the 3–6 $Å^{-1}$ range, when manganese atoms are introduced in the first coordination shell. This is precisely the range where this element contributes significantly to the signal amplitude. Actually, the Q factor decreases respectively from 9 and 11% without Mn atoms, which are relatively poor values, to 3.5 and 2.5%, for the $Pd_{90}Mn_{10}$ and $Pd_{65}Mn_{35}$ catalysts, respectively.

The Pd-Pd distances reported in Table 3 range from 2.73 to 2.81 Å. They vary not only with the alloy composition but also significantly with the mode of activation. This may seem surprising, but the crystallographic data reported in Table 4 show that different ordered Pd-Mn alloys with the AuCu and CsCl structures also exhibit distances differing by 0.15 Å.

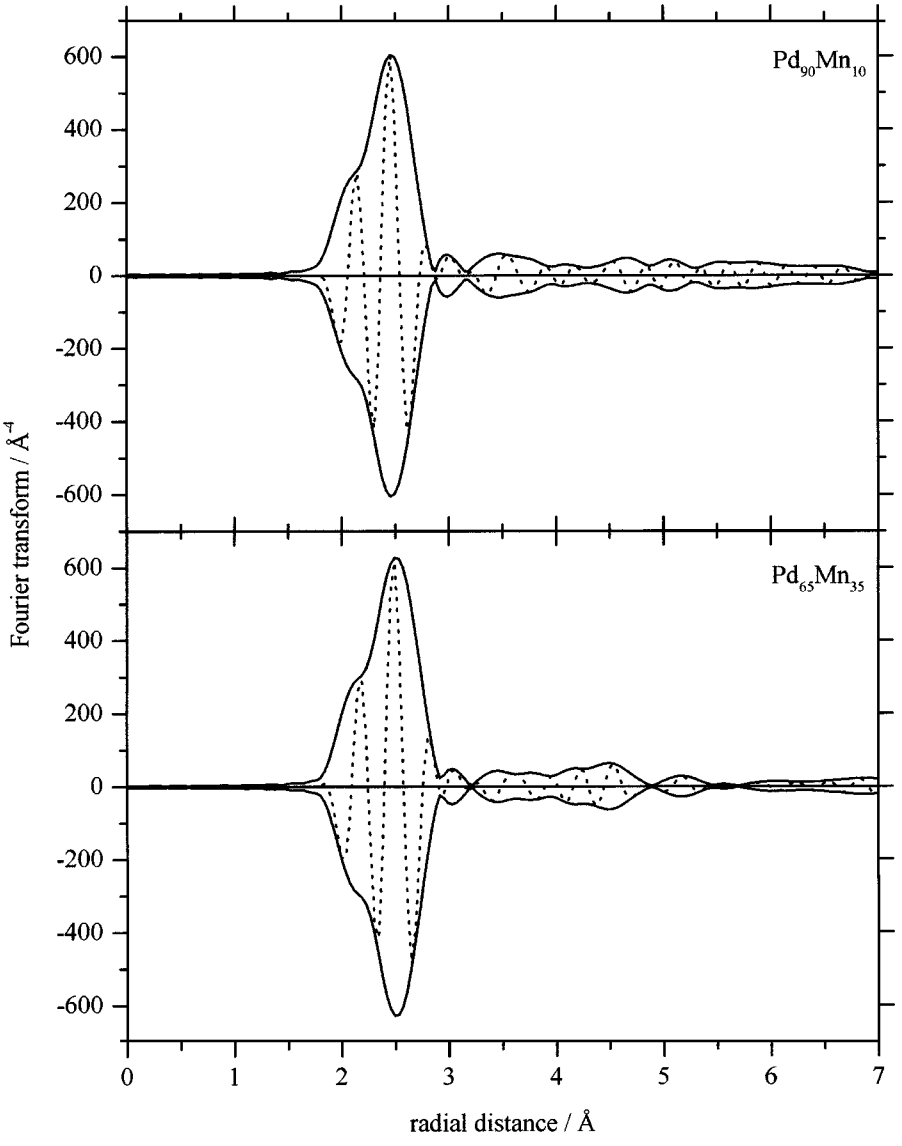

FIG. 13. Magnitudes and imaginary parts of the FTs of the EXAFS spectra of $Pd_{65}Mn_{35}/SiO_2$ and $Pd_{90}Mn_{10}/SiO_2$ at the Pd K-edge.

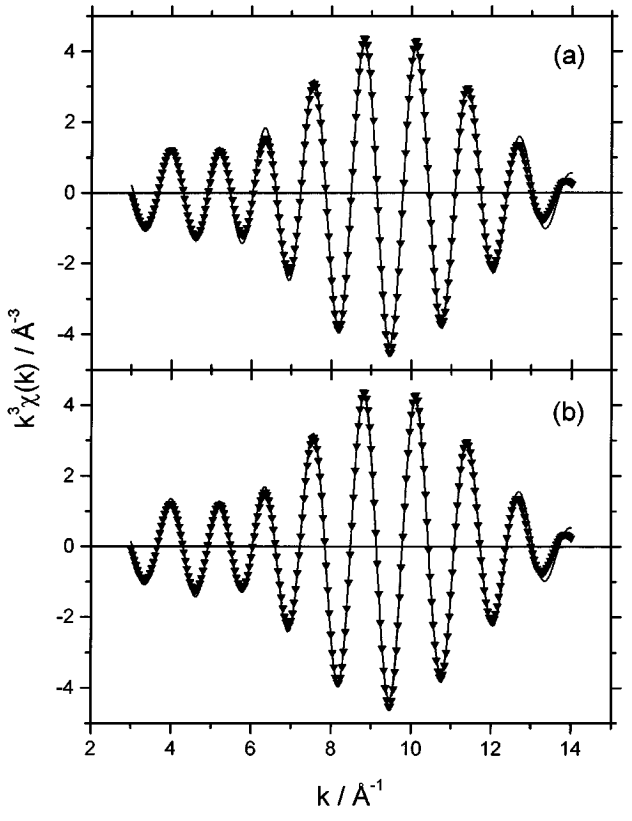

FIG. 14. EXAFS data for $Pd_{65}Mn_{35}/SiO_2$ bimetallic sample at the Pd K-edge: (a) first shell experimental (triangles) and modeled (solid line) contribution with only Pd atoms; (b) first shell experimental (triangles) and modeled (solid line) contribution with both Pd and Mn atoms.

Similarly, if the experimental Pd-Mn distances are found to vary from 2.70 to 2.79 Å, it is observed that Pd-Mn bonds also extend from 2.37 to 2.85 Å in the ordered compounds. As shown by EDX the composition of bimetallic particles may vary from one bimetallic catalyst to the other and from one particle to the other. This may explain the variation of interatomic distance measured by EXAFS.

TABLE 3

EXAFS Results for the Bimetallic Catalysts

Sample/ treatment	Pair	n	R (Å)	$\Delta\sigma^2$ (Å^2)	ΔR (Å)	Δk (Å^{-1})	Q (%)
Pd/SiO_2	Pd-Pd	10.7	2.75	0.004	1.65–2.95	2.4–14	6
$Pd_{90}Mn_{10}$	Pd-Pd	8.5	2.71	0.010	1.65–2.95	2.4–14	30
argon 770 K	Pd-Pd	10.2	2.73	0.007	1.65–2.95	2.4–14	14
	Pd-Mn	0.2	2.70	0.001			
$Pd_{90}Mn_{10}$	Pd-Pd	11.3	2.77	0.001	1.6–2.9	2.4–14	9
calc. 720 K,	Pd-Pd	12.0	2.76	0.002	1.6–2.9	2.4–14	3.5
red. 870 K	Pd-Mn	0.3	2.71	0.001			
$Pd_{65}Mn_{35}$	Pd-Pd	8.5	2.81	0.001	1.6–2.9	2.4–14	11
calc. 720 K,	Pd-Pd	9.7	2.81	0.002	1.6–2.9	2.4–14	2.5
red. 870 K	Pd-Mn	1.4	2.79	0.002			

Note. The EXAFS data were modeled with and without Mn atoms in the first coordination shell of palladium.

TABLE 4

Crystallographic Data for Various Pd-Mn Alloys

Alloy (structure reference)	Pd-Pd (Å)	Pd-Mn (Å)	Reference
PdMn (AuCu type)	2.88	2.71	(15)
PdMn (CsCl type)	2.733	2.367	(11)
Pd_3Mn (Au_3Pd type)	2.755	2.767	(14)
$Pd_{21}Mn_{11}$	2.724	2.85	(15)

The large values of the total coordination numbers, comprised between 11 and 12, confirms the formation of large particles in the case of the calcination/reduction treatment, whereas this value is only 10 for the samples decomposed at 770 K under argon, in agreement with the presence of 3-nm particles.

4. CONCLUSION

The present study has shown that, contrary to the case of $Pd(acac)_2$ and $Cu(acac)_2$, Pd-Mn mixed molecular complexes cannot be synthesized by exchange/deposition on the silica support because of the different mode of anchoring these two molecules. The Pd complex has a weak interaction with silica, compared to alumina, and this limits the exchange capacity to 2–3 wt%. On the contrary, a chemical reaction occurs between the silanol groups of the support and the Mn acetylacetonate complex, leading to its partial decomposition during the exchange.

EDX operated in scanning mode on a large area of the catalysts obtained either by decomposition under argon or by calcination/reduction of the supported complexes, has shown that manganese is well dispersed on the support, forming a thin layer; but it has also shown the formation of bimetallic particles by observations in the spot mode.

The XANES studies at the Mn K-edge demonstrate that most of this element is nonmetallic and remains mainly under an oxidized state, even if the spectra are different from that of MnO_2. This is why an EXAFS experiment at the Mn K-edge was estimated to be purposeless.

After decomposition of the complexes and reduction, as shown in Table 5 which summarizes the results, analytical microscopy confirms that all the particles contain a small

TABLE 5

Comparison between EM, EDX, and EXAFS

Sample	EM d_s (nm)	EDX Pd at%	EXAFS Pd at%
$Pd_{90}Mn_{10}$	5	95	98
$Pd_{65}Mn_{35}$	4.9	75	87

Note. Results on individual particles for bimetallic catalysts (calcination/reduction treatment).

proportion of manganese, 4 to 5% for the $Pd_{90}Mn_{10}$ catalyst and 20 to 25% for the $Pd_{65}Mn_{35}$ sample. If one compares these values to the ratio of the Pd-Mn to the Pd-Pd coordination numbers measured by EXAFS, one concludes that approximately half of this manganese contained in a particle is metallic and alloyed to palladium. The remaining manganese, in the oxidic form, partially covers the particles of alloy and the support.

More work is still necessary to understand how this complex system interacts with molecules like CO and NO and can promote the conversion of their mixture (3).

ACKNOWLEDGMENT

The authors are indebted to the Laboratoire pour l'Utilisation du Rayonnement Électromagnétique (LURE-Orsay) for dedicated runs and lending of the EXAFS ovens.

REFERENCES

1. Borgna, A., Moraweck, B., Massardier, J., and Renouprez, A. J., *J. Catal.* **128**, 99 (1991).
2. Mergler, Y. J., van Aalst, A., van Delft, J., and Nieuwenhuis, B. E., *J. Catal.* **161**, 310 (1996).
3. Trillat, J. F., Massardier, J., Moraweck, B., Praliaud, H., and Renouprez, A. J., *in* "Fourth International Congress on Catalysis and Automotive Pollution Control, CAPOC4, Brussels, April, 1997" (N. Kruse, A. Frennet, and J.-M. Bastin, Eds.), Vol. 2, p. 23.
4. Renouprez, A., Lebas, K., and Bergeret, G., *J. Molec. Cat. A* **120**, 217 (1997).
5. Faudon, J. F., Senocq, F., Bergeret, G., Moraweck, B., Clugnet, G., and Renouprez, A., *J. Catal.* **144**, 460 (1993).
6. Rousset, J. L., Cadrot, A. M., Cadete Santos Aires, F. J., Renouprez, A., Mélinon, P., Perez, A., Pellarin, M., Vialle, J. L., and Broyer, M., *J. Chem. Phys.* **102**, 8574 (1995).
7. Moraweck, B., and Renouprez, A., *Surf. Sci.* **111**, 53 (1981).
8. Nelder, J. A., and Mead, R., *Comput. J.* **7**, 308 (1965).
9. Stern, E. A., *Phys. Rev. B* **48**, 9825 (1993).
10. Rehr, J. J., and Albers, R. C., *Phys. Rev. B* **41**, 8139 (1990).
11. Raub, E., and Mahler, W., *Z. Metallk.* **45**, 430 (1954).
12. Lytle, F. W., Greegor, R. B., Via, G. H., and Sinfelt, J. H., *J. Chem. Phys.* **70**, 4849 (1979).
13. Vasudevan, thesis, Institut Français du Pétrole, Technip, Paris, 1982.
14. Iwasaki, H., Okamura, K., and Ogawa, S., *J. Phys. Soc. Jpn* **31**, 497 (1971).
15. Kjekshus, A., Mollerud, R., Andresen, A. P., and Pearson, W. B., *Phil. Mag.* **16**, 1063 (1967).